SUPPLEMENTARY MATERIAL

Supplementary Methods

Supplementary Tables

Table S1 (separate Excel file): Liquid chromatography tandem mass spectrometry analysis of proteins co-immunoprecipitating with endogenous NPM1/mutated-NPM1 from nuclear and cytoplasmic fractions of *NPM1*-wildtype (THP1) and *NPM1*-mutated AML cells (OCI-AML3).

Table S2 (separate Excel file): MYC target genes identified from the literature (~300 genes to which MYC directly binds in chromatin immunoprecipitation analyses).

Table S3 (separate Excel file): Myeloid commitment genes (~200 genes significantly upregulated in CMP/GMP *vs* HSC).

Table S4 (separate Excel file): Monocyte differentiation genes (~300 genes significantly upregulated in monocytes *vs* HSC, CMP and GMP).

Table S5 (separate Excel file): Granulocyte differentiation genes (~300 genes significantly upregulated in granulocytes *vs* HSC, CMP and GMP).

Table S6 (separate Excel file): Liquid chromatography tandem mass spectrometry analysis of proteins co-immunoprecipitating with endogenous CEBPA from nuclear fractions of *NPM1*-mutated AML cells (OCI-AML3).

Table S7 (separate Excel file): Liquid chromatography tandem mass spectrometry analysis of proteins co-immunoprecipitating with endogenous RUNX1 from nuclear fractions of *NPM1*-mutated AML cells (OCI-AML3).

Supplementary Figures

Figure S1. Reverse immunoprecipitation showing NPM1 was pulled down with PU.1.

Figure S2. Secondary antibody controls for immunofluorescence microscopy experiments.

Figure S3. The master transcription factor expression pattern of AML cells resembled that of normal GMP/monocytes, and not that of normal HSC.

Figure S4. Pu.1 binds at monocyte- and granulocyte-differentiation genes but not myeloid-commitment genes.

Figure S5: Validation in our separate database of gene expression during normal hematopoiesis, that the MYC-target, myeloid-commitment and monocyte-differentiation gene sets identified by analysis of GSE24759 (51) cluster together in hierarchical clustering analyses, and reliably discriminate between HSC, committed myeloid progenitors, granulocytes and monocytes.

Figure S6: There is an inverse correlation in MYC-target and monocyte differentiation gene expression in AML cells.

Figure S7. Pu.1 nuclear relocation in Pu.1-null myeloid precursors represses key precursor genes (e.g., *Hoxa9*) and activates terminal monocytic fates.

Figure S8. Selinexor induces monocytic differentiation in *NPM1*-mutated AML cells, while decitabine induces monocytic and granulocytic differentiation in *NPM1*-mutated and *NPM1*-wildtype AML cells.

Figure S9: Low nanomolar (10, 50 nM) concentrations of selinexor (KPT330) that induce monocytic differentiation of *NPM1*-mutated AML cells do not induce early apoptosis.

Figure S10. Selinexor (KPT330) at a non-toxic dose significantly decreased AML burden in a patient-derived xenotransplant model of dual *NPM1*/*FLT3*-mutated AML.

Figure S11. Monocyte and granulocyte terminal-differentiation genes, but not commitment/proliferation genes, are suppressed in cytogenetically normal AML cells (n=100) compared to normal granulocytes and monocytes.

Figure S12. Coregulator interactions of nuclear RUNX1 in *NPM1*-mutated AML cells before and after DNMT1-depletion or PU.1 nuclear retention.

Figure S13. Granulocyte lineage-differentiation, and DNMT1-depletion from *NPM1*-mutated AML cells by decitabine, decrease NPM1 protein levels and increase PU.1 nuclear location.

Figure S14. Human and murine CD45 expression in bone marrow cells obtained from mice at time-of-distress.

Figure S15. Cell cycle distribution of bone marrow AML cells obtained from mice at time-of-distress.

Figure S16. Monocyte (CD14) and granulocyte (CD11b) lineage-differentiation marker expression in bone marrow cells obtained from mice at time-of-distress.

Figure S17. CD14-positive *NPM1*-mutated AML cells did not stain for CD11b or CD15 (monocytic), while CD14-negative *NPM1*-mutated AML cells co-stained for CD11b and CD15 (granulocytic).

Figure S18. γ-H2AX expression as a marker for apoptosis/DNA damage in bone marrow cells obtained from mice at time-of-distress.

Figure S19. Resistance both in vivo and in vitro was by preventing target-engagement. A) NPM1 and PU.1 localization in *NPM1*/*FLT3*-mutated AML cells harvested from murine bone marrow at the time-of-distress.

SUPPLEMENTARY METHODS

***Cell fractionation, nuclear protein extraction, covalent binding of antibodies to protein A/G beads, immunoprecipitation, 1D SDS-polyacrylamide gel electrophoresis and Western blot analysis*.** As we have previously described (21). Antibodies used were mouse anti-NPM1 (SCBT, SC-47725); rabbit anti-CEBPA (PROTEINTECH, 18311-1-AP); mouse anti-RUNX1 (SCBT, sc-101146); anti-mutant-NPM1 (PA1-46356, Thermo Scientific); secondary antibodies - anti–rabbit (GE Healthcare, NA934) and anti–mouse (GE Healthcare, NXA931)(used at 1:5000 and 1:10 000 dilutions, respectively).

Co-transfection of HEK293 cells with expression vectors for NPM1, mutated NPM1 and PU.1. Human sequences for wild-type *NPM1*, mutated *NPM1* (exon 12, TCTG insertion) and PU.1, were cloned into pCSTAP2 (AddGene) containing N-terminal FLAG-tag and co-transfected into human embryonic kidney (HEK-293, ATCC) cells. After 48 hours of culture on coverslips, cells were imaged by immunofluorescence as described above.

***NanoLC-ESI-LTQ-Orbitrap MS/MS*.** Immunoprecipitation products were subjected to SDS-polyacrylamide gel electrophoresis and stained with colloidal Coomassie Blue (Gel Code Blue, Pierce Chemical). Gel slices were excised from the top to the bottom of the lane; proteins were reduced with dithiothreitol (Sigma-Aldrich, D0632, 10mM), alkylated with iodoacetamide (Sigma-Aldrich, I1149, 55mM), and digested in situ with trypsin. Peptides were extracted from gel pieces 3 times using 60% acetonitrile and 0.1% formic acid/water. The dried tryptic peptide mixture was redissolved in 20 µL of 1% formic acid for mass spectrometric analysis. Tryptic peptide mixtures were analyzed by on-line LC-coupled tandem mass spectrometry (LC-MS/MS) on an Orbitrap mass spectrometer (Theomo Fisher Scientific).

Database Search and Data Validation. Mascot Daemon software (version 2.3.2; Matrix Science, London, UK) was used to perform database searches, using the Extract_msn.exe macro provided with Xcalibur (version 2.0 SR2; Thermo Fisher Scientific) to generate peaklists. The following parameters were set for creation of the peaklists: parent ions in the mass range 400–4500, no grouping of MS/MS scans, and threshold at 1000. A peaklist was created for each analyzed fraction (i.e., gel slice), and individual Mascot (version 2.3.01) searches were performed for each fraction. The data were searched against Homo sapiens entries in Uniprot protein database (Feb 2018 release; 20,316 total sequences). Carbamidomethylation of cysteines was set as a fixed modification, and oxidation of methionine was set as a variable modification. Specificity of trypsin digestion was set for cleavage after Lys or Arg, and two missed trypsin cleavage sites were allowed. The mass tolerances in MS and MS/MS were set to 10 ppm and 0.6 Da, respectively, and the instrument setting was specified as “ESI-Trap.” To calculate the false discovery rate (FDR), the search was performed using the “decoy” option in Mascot. The spectral FDR and protein FDR are 0.35±0.17 % and 4.28±1.99 % respectively. A minimum Mascot ion score of 25 and peptide rank 1 was used for automatically accepting all peptide MS/MS spectra.

Label free relative protein quantitation (LFQ). Relative protein quantification was performed using spectral count-based LFQ. For each biological sample, data from the individual gel slices were combined. Statistical analysis was performed on all proteins identified with average spectral counts of ≥2 of at least one of the three experiments. The spectral count data was normalized by total spectral counts of the bait protein (NPM1, CEBPA, or RUNX1) in each sample to adjust for differences in overall protein levels among samples. Proteins were considered to have a significant difference in abundance if there was a difference of twofold or greater in normalized spectral counts between experiments and a p value ≤ 0.01 using a two-tailed t test. Spectral counts for all proteins and peptides identified are provided in supplementary material.

Giemsa staining of cells. Cytospins of cells from bone marrow or peripheral blood were fixed for 2 minutes in methanol, air-dried, and stained for 20 minutes with filtered modified solution of Giemsa stain (Sigma Aldrich, Cat # 48900, St Louis, MO), diluted (1:20) with buffer solution pH6.5, rinsed with distilled water, air-dried and examined using low and high magnifications with a Leica DMR microscope (Leica Microsystems, Wetzlar GmbH, Germany) connected to Nuance multispectral imaging system FX using Nuance version 3.0.2 software (PerknElmer, Inc., Hopkinton, MA).

Flow Cytometry Analyses for CD14, CD11b, CD15 and γH2AX. As we have previously described (20, 21). Antibodies used were anti-human CD14 (clone: M5E2, cat. no. 301850, Biolegend, San Diego, CA, 1:100), anti-human CD11b (clone: M1/70, cat. no. 101206, Biolegend, 1:100), anti-human CD15 (clone: HI98, cat. no. 301903, Biolegend, 1:100), monoclonal anti-human CD45 (clone HI30, cat. No 304016, Biolegend, 1:100), monoclonal anti-mouse CD45 (Clone 30-F11, cat. No 1031066, Biolegend, 1:100), and anti-γH2AX (Clone N1-431, cat. no. 560445, BP Bioscience, 1:100).

Flow cytometry to measure cell cycle distribution. Bone marrow cells were washed in PBS then fixed in cold 70% ethanol for 30 minutes at 4°C, added drop wise to the pellet while vortexing, to ensure fixation of all cells and to minimize clumping. The fixed cells were washed twice in PBS followed by addition of 50 µl of a 100 µg/ml stock of RNase, to ensure only DNA, and not RNA, was stained (100 µg/ml RNase DNase free, Promega, Ref #A797C). DNA was stained using 200 µl of PI/Triton-X100 staining solution: 12.5 mg (50 µg/ml) propidium iodide (Molecular Probe), 250 mg Na Citrate (Sigma), and 250 ul Triton X-100 (Sigma), in distilled water 250 mL, prepared freshly and stored in the dark at 4°C. Acquistion analysis used a Cytomics FC500 Flow Cytometer System with Software CXP (Beckman Coulter). Forward scatter (FSc) and side scatter (SSc) was used to exclude debris and cell doublets. Gating on singlets used FL3 lin (H) *vs* PI integral (AUX) followed by gating for cell cycle phases: sub-G1, G0/G1, S phase, and G2/M.

***Apoptosis detection*.** Apoptosis was detected by Annexin-V and 7AAD co-staining using the APOAF commercial kit (Sigma). Cells ($5x10^5$) were washed and incubated for 30 minutes with FITC-conjugated Annexin-V at room temperature. Cells were then resuspended in 400 mL of binding buffer containing 7AAD and immediately analyzed by flow cytometry.

Culture and differentiation of Pu.1-ER cells. Pu.1-ER cells (PUER) are murine hematopoietic precursor cells that have been retrovirally transduced to express PU.1 fused to the estrogen receptor (gift of Dr. Harinder Singh (53)). PUER cells were grown in Iscove's modified Eagle's medium, without phenol-red, with 10% fetal bovine serum, 5 ng/ml mIL-3, 1µg/ml Puromycin, 55µM beta-ME, 1% penicillin/streptomycin at 37°C in a humidified atmosphere with 5% CO2 in air. Addition of the estrogen agonist 4-hydroxy-tamoxifen (OHT) to PUER triggers their terminal differentiation into macrophages (53).

DNA isolation, reverse transcription (RT) and real-time PCR. DNA isolation, reverse transcription (RT) and real-time PCR. Total RNA from cultured cells was isolated using NucleoSpin® RNA (Clontech, Cat# 740984.5) according to the manufacturer's instruction. The cDNA was then synthesized from total RNA using the iScript cDNA synthesis Kit (BioRad, Cat# 1708891). Quantitative gene expression levels were detected using real-time PCR with the ABI PRISM 7500 Fast Sequence Detection System and SYBR Advantage qPCR Premix (Clontech, 639676) according to the manufacturer's instructions. Primers for all genes analyzed were purchased from Integrated DNA Technologies (primer sequences are provided in supplementary material). Relative expression values (RQ values) were calculated by the delta-delta C_T method with beta-actin or GAPDH as the internal control.

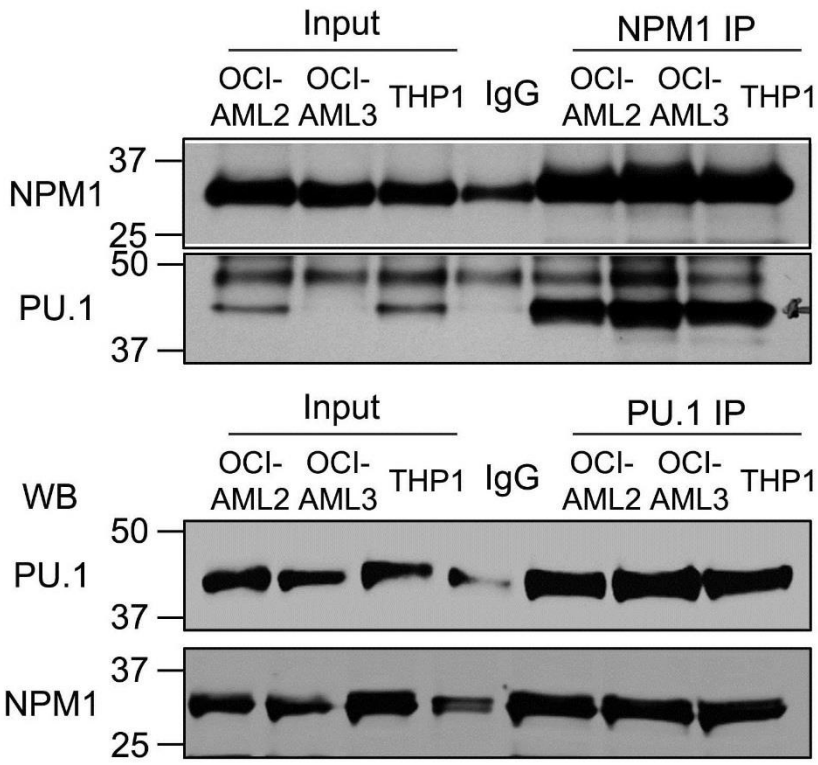

Figure S1. Bi-directional immunoprecipitations showing PU.1 pull-down with NPM1 and NPM1 pull-down with PU.1. PU.1 or NPM1 were immunoprecipitated from whole cell lysates of *NPM1*-wildtype (OCI-AML2, THP1) and *NPM1*-mutated (OCI-AML3) AML cells, with control immunoprecipitations using isotype IgG. Western blots for PU.1 and NPM1.

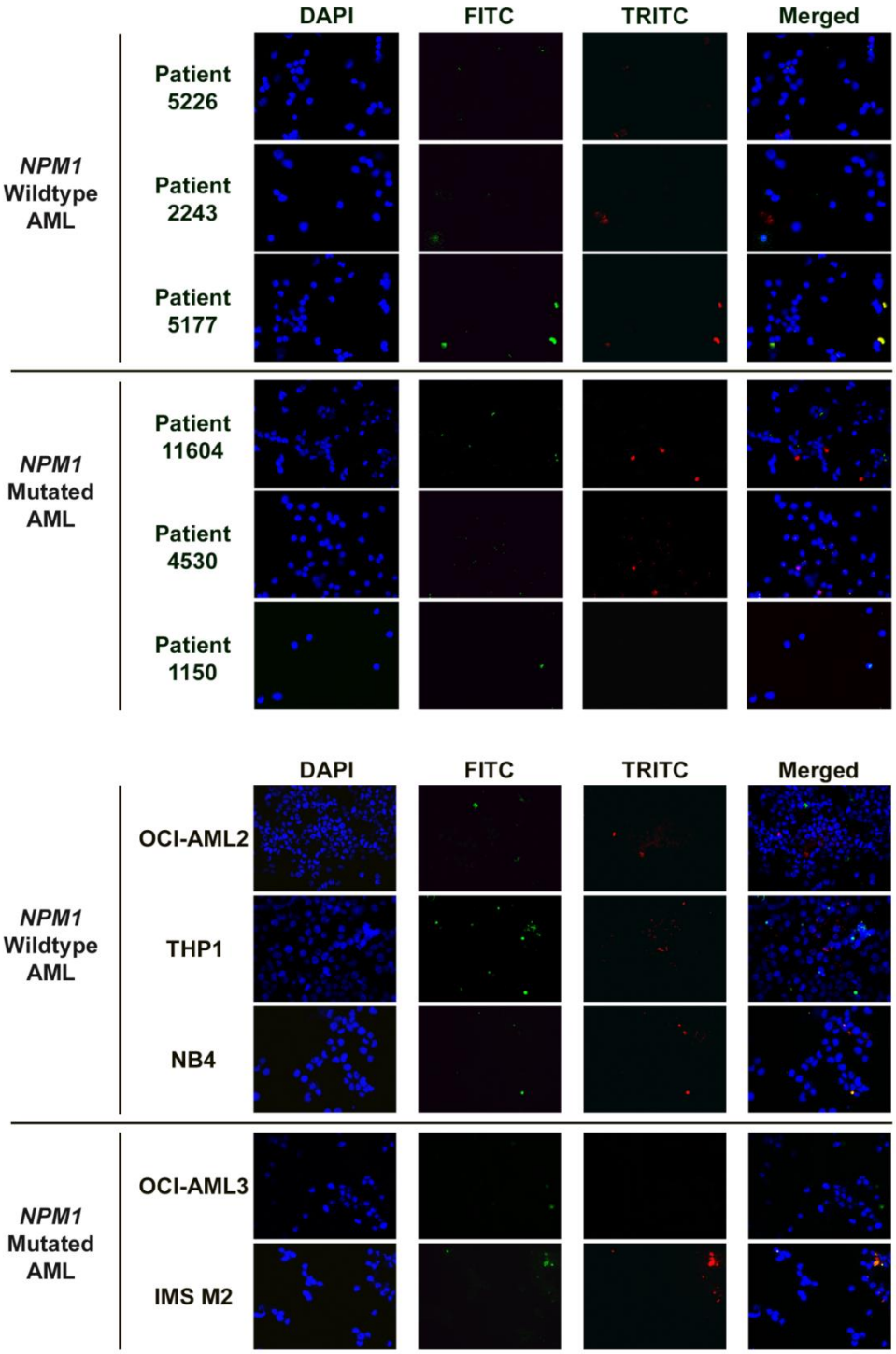

Figure S2. Secondary antibody controls for immunofluorescence microscopy experiments. AML cell lines and AML primary cells were stained with secondary antibodies, Alexa Fluor 488 Goat Anti-Mouse (FITC) or Alexa Fluor 568 Goat Anti-Rabbit IgG (TRITC), only. DAPI was used to stain nuclei. Images were taken with Nikon Eclipse 400 microscope. Magnification 630X.

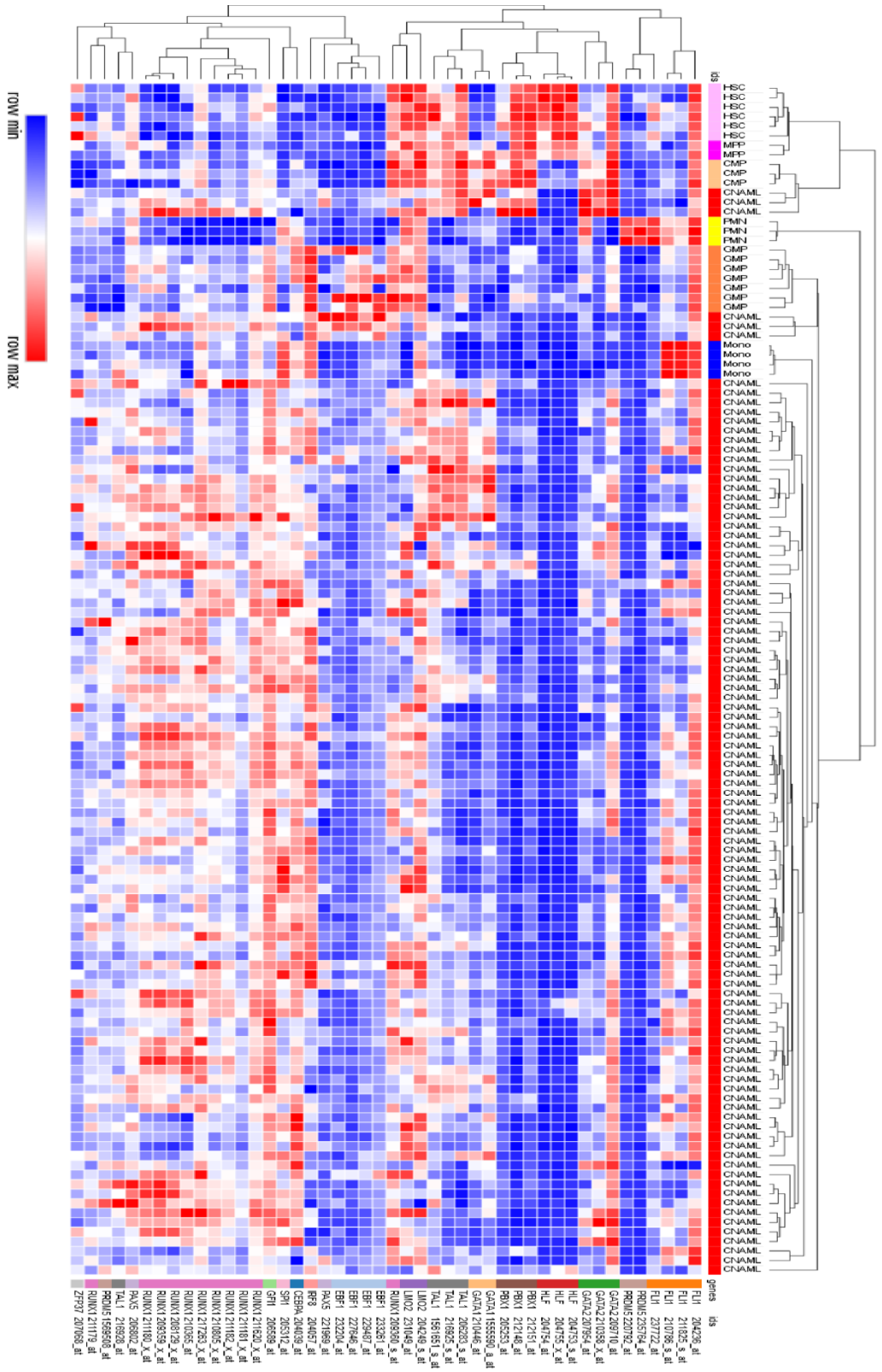

Figure S3. The master transcription factor expression pattern of AML cells (SPI1, RUNX1, CEBPA, IRF8, GFI1, GATA1, GATA2, FLI1, TAL1, LMO2, EBF1, PAX5, HLF, PBX1, PRDM5, ZFP37) resembled that of normal GMP/monocytes, and not that of normal HSC. Results of unbiased hierarchical clustering analyses – one minus Pearson correlation with average linkage method – indicated on right. Heat map generated using Morpheus (Broad Institute, Boston, USA). Gene expression was curated as described in Methods.

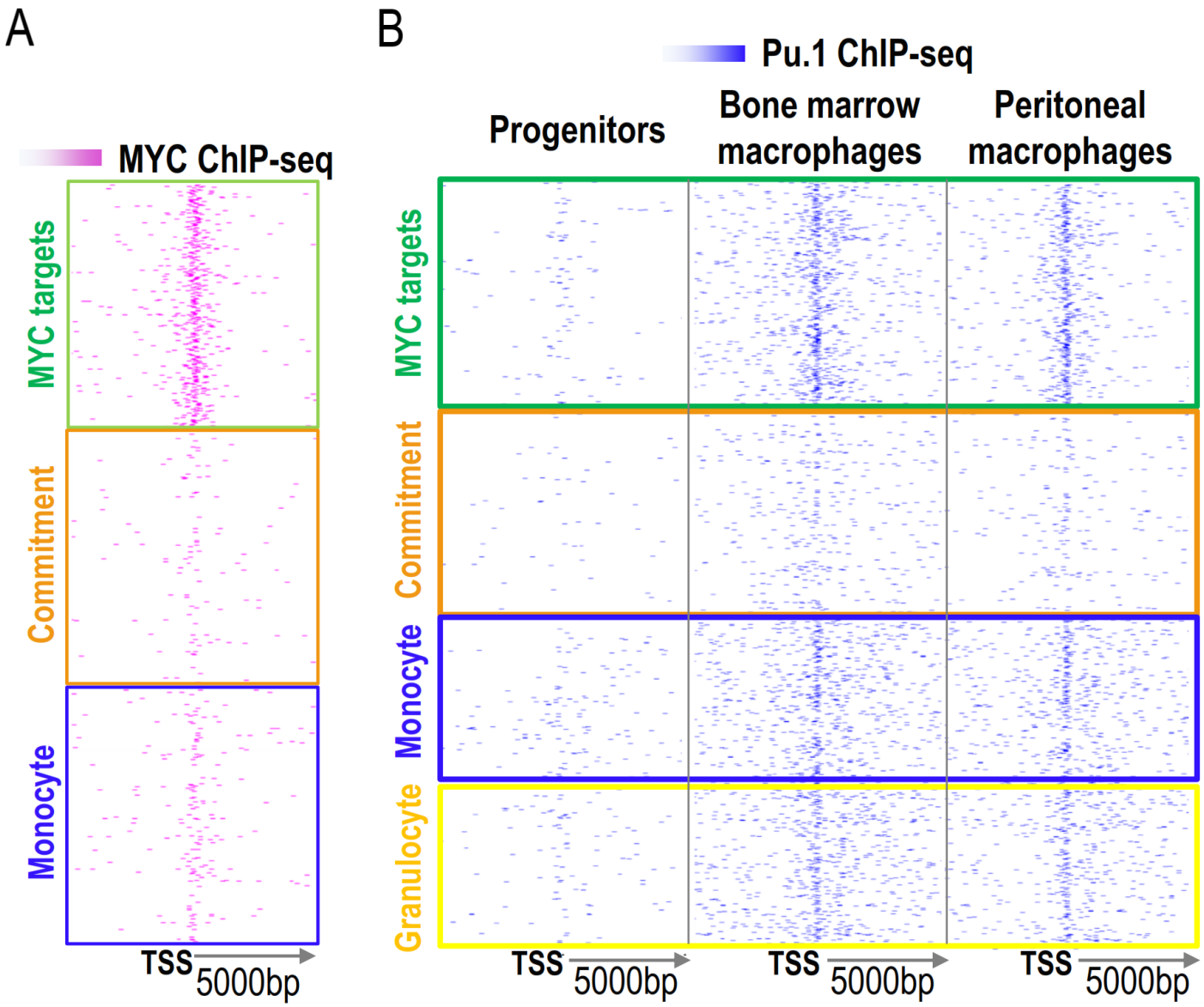

Figure S4. Pu.1 binds at monocyte- and granulocyte-differentiation genes but not myeloid-commitment genes. GEO Database numbers for ChIP-Seq values analyzed are listed in Methods. **A) Validation of MYC target genes using ChIP-seq data from Encode.** MYC ChIP-seq in K562 AML cells. Aligned ChIP-Seq reads visualized using Easeq (97), with values normalized to reads per million per 1kbp. **B) Pu.1 binds to monocyte-, granulocyte-differentiation, and Myc-target genes, but not myeloid-commitment genes**. MYC targets, myeloid-commitment, monocyte-differentiation and granulocyte-differentiation genes were identified as per figure 2 and Methods. Pu.1 ChIP-Seq in primary murine bone marrow and peritoneal macrophages (52).

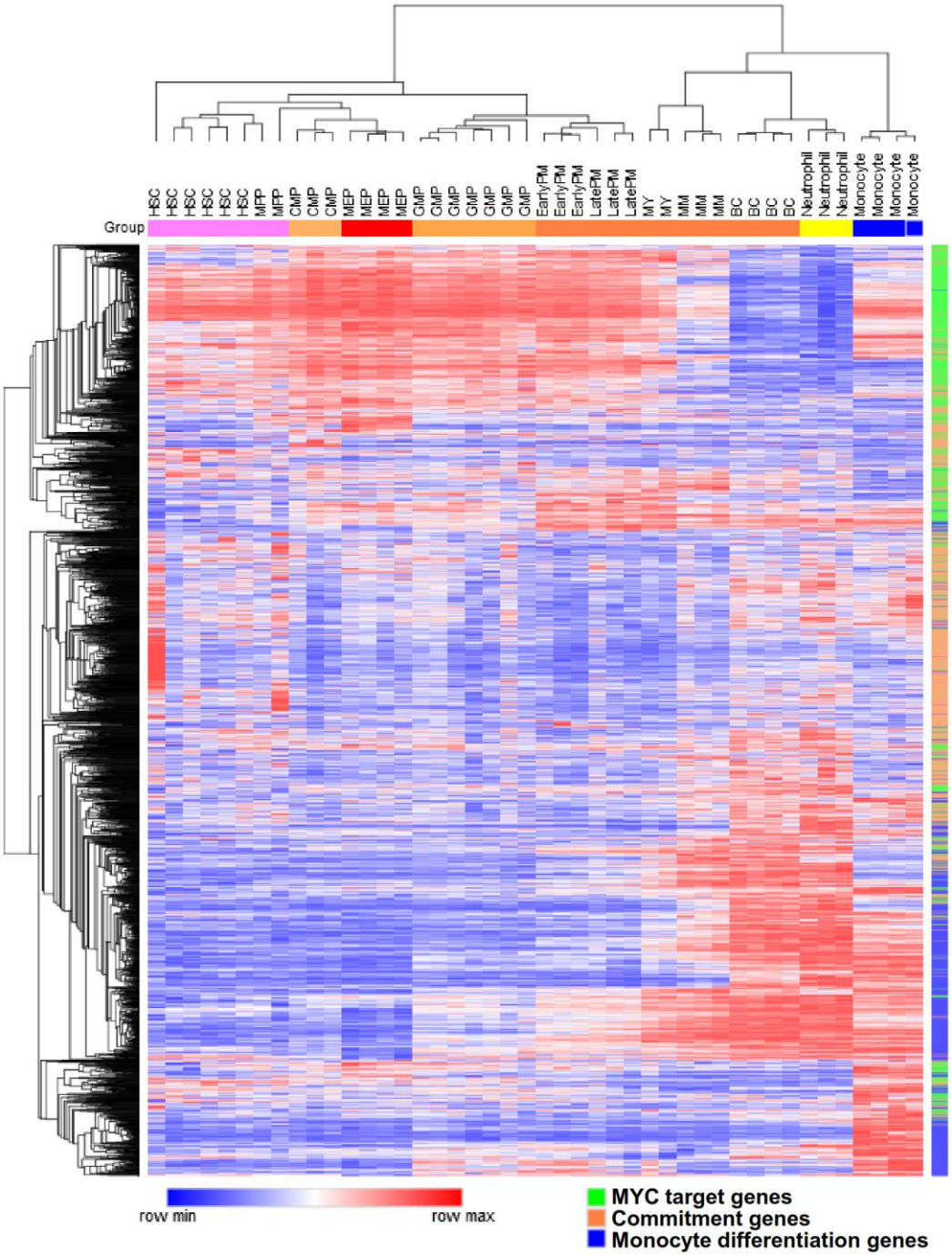

Figure S5: Validation in our separate database of gene expression during normal hematopoiesis, that the MYC-target, myeloid-commitment and monocyte-differentiation gene sets identified by analysis of GSE24759 (51) cluster together in hierarchical clustering analyses, and reliably discriminate between HSC, committed myeloid progenitors, granulocytes and monocytes.

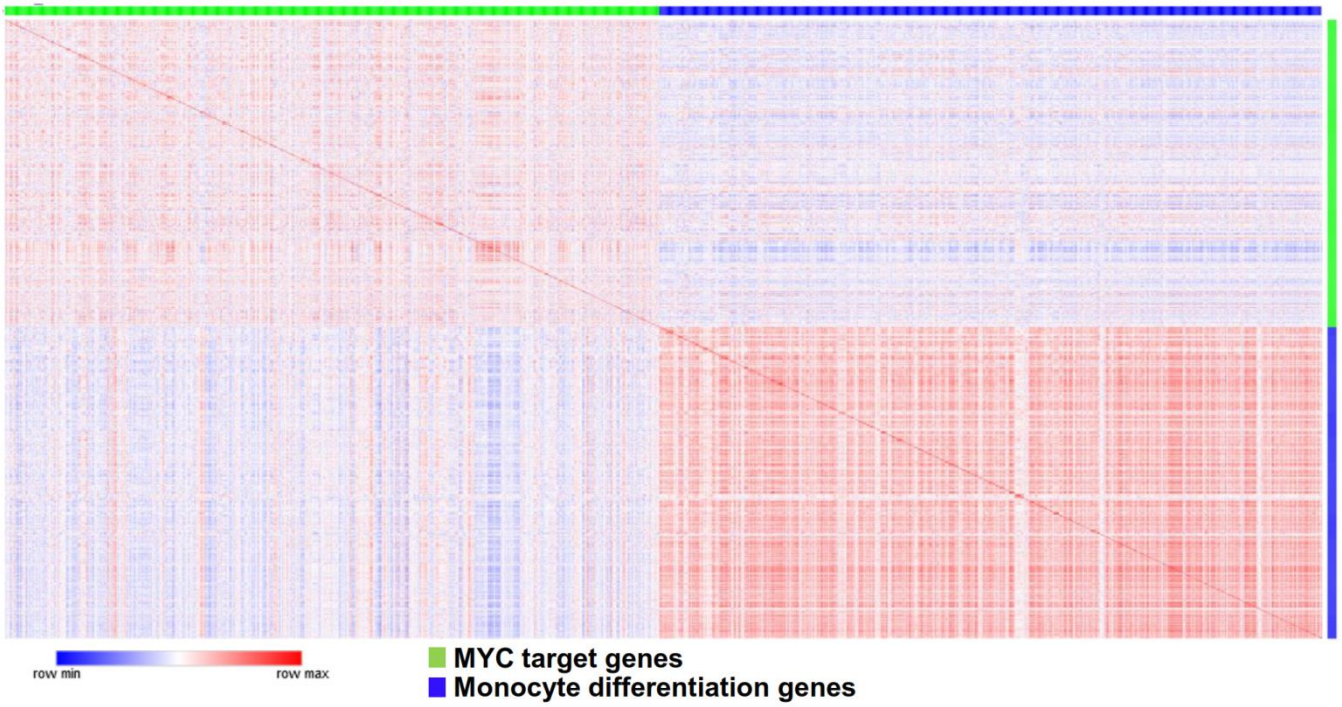

Figure S6: There is an inverse correlation in MYC-target and monocyte differentiation gene expression in AML cells. The heatmap indicates the size of the Pearson correlation coefficients of MYC-target and monocyte-differentiation genes in CNAML (n=989) with the blue colors in the heatmap indicating negative correlation coefficient values, and red colors positive correlation coefficient values, between these two gene sets. Heatmap generated with the Similarity Matrix tool in Morpheus (Broad Institute).

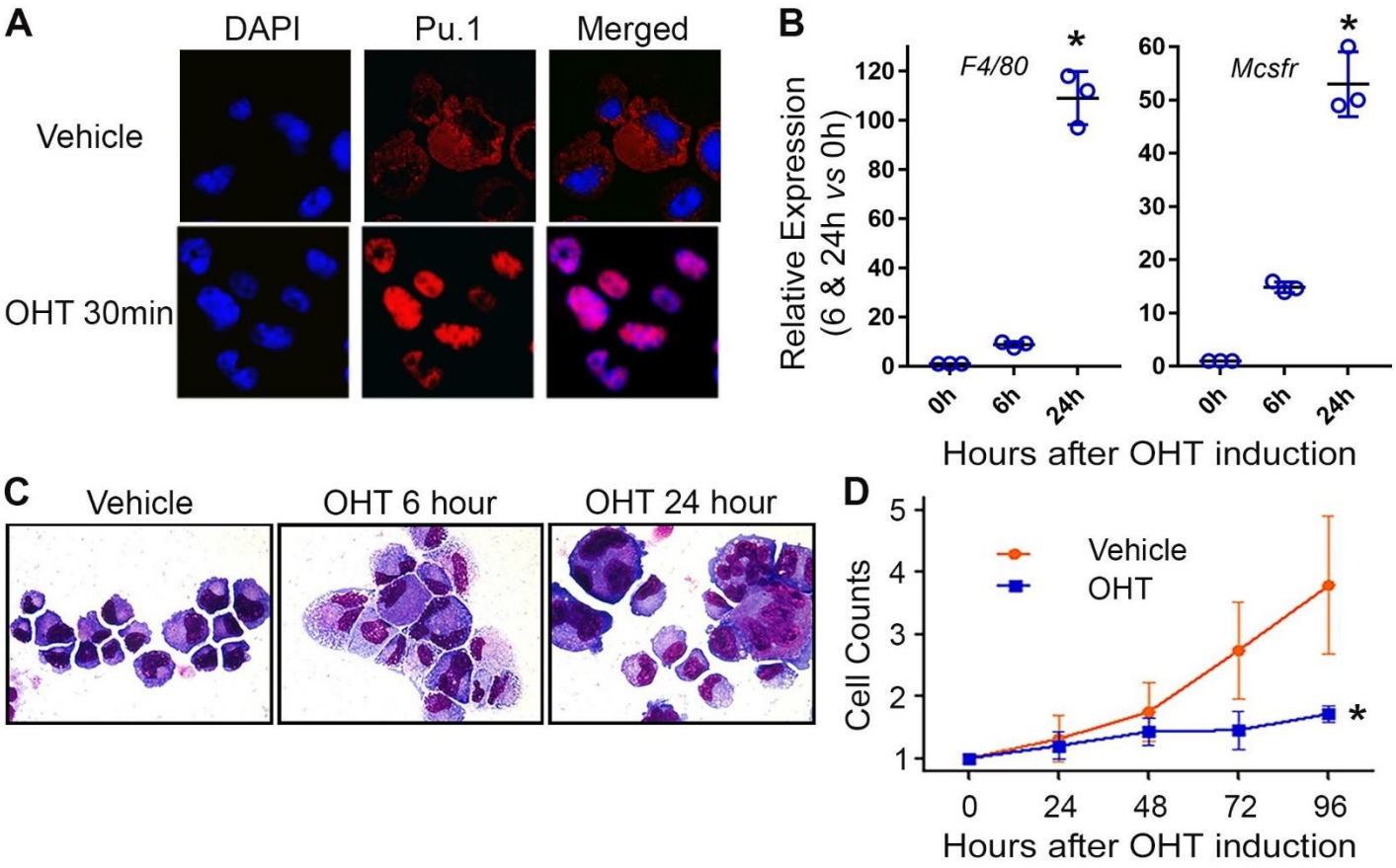

Figure S7. Pu.1 nuclear relocation in Pu.1-null myeloid precursors represses key precursor genes (e.g., *Hoxa9*) and activates terminal monocytic fates (supplement to figure 3). A) Addition of estrogen (OHT) translocates Pu.1 into the nucleus in Pu.1-knockout (Pu.1$^{-/-}$) myeloid precursors retrovirally transduced to express Pu.1 fused with the estrogen receptor (Pu.1-ER) (53). **B) QRT-PCR for terminal monocytic differentiation markers** F4/80 and macrophage colony stimulating factor (Mcsfr, Csf1r) expression relative to 0 hours, beta-actin internal control. Mean±SD three independent experiments.*p<0.01 2-sided t-test 24h *vs* 0h. **D) Cell morphology**. Giemsa-stain. Leica DMR microscope, 630X. **D) Cell counts** x10^6, by automated cell counter. Mean±SD three independent experiments. *p<0.01 2-sided t-test OHT *vs* Veh at 96h.

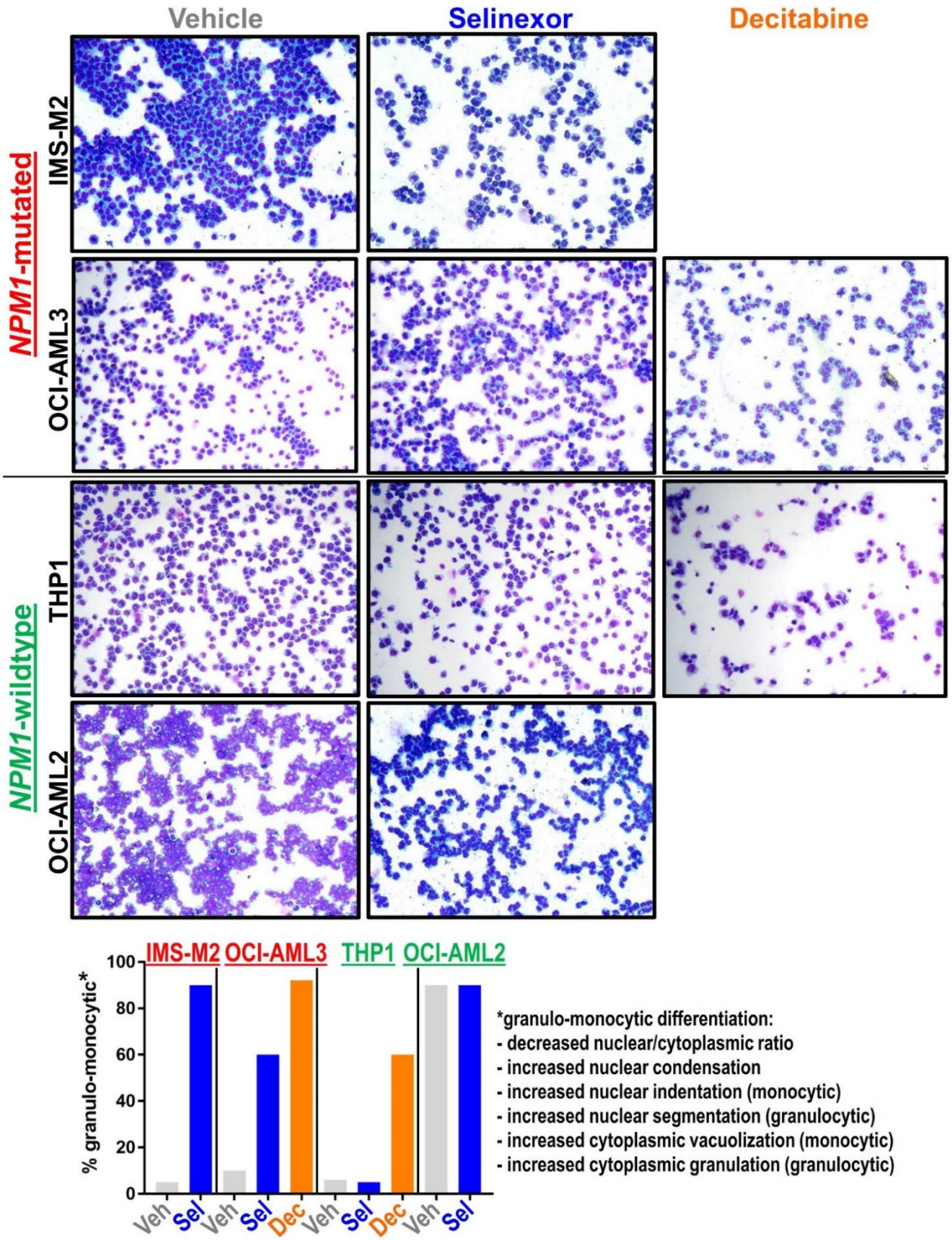

Figure S8. Selinexor induces monocytic differentiation in *NPM1*-mutated AML cells, while decitabine induces monocytic and granulocytic differentiation in *NPM1*-mutated and *NPM1*-wildtype AML cells. Day 4. Giemsa-stain. Percentage granulo-monocytic based on listed features derived from counting 100 cells. Representative fields shown. The decitabine-treated OCI-AML3 photomicrograph is a wider-field version of the same photomicrograph in **Figure 5B**. Leica DMR microscope, 100X (supplement to figures 5 and 9).

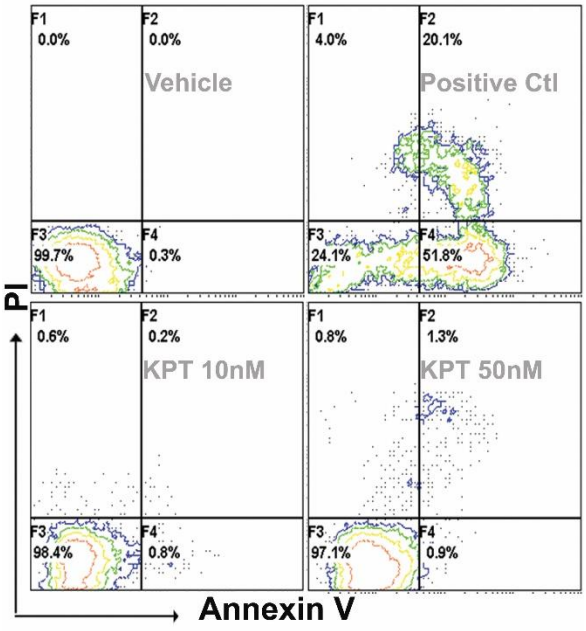

Figure S9: Low nanomolar (10, 50 nM) concentrations of selinexor (KPT330) that induce monocytic differentiation of *NPM1*-mutated AML cells do not induce early apoptosis. Flow cytometry for PI and Annexin-FITC staining 24 hours after addition of vehicle, selinexor at the indicated concentrations or camptothecin 3 µM as a positive control.

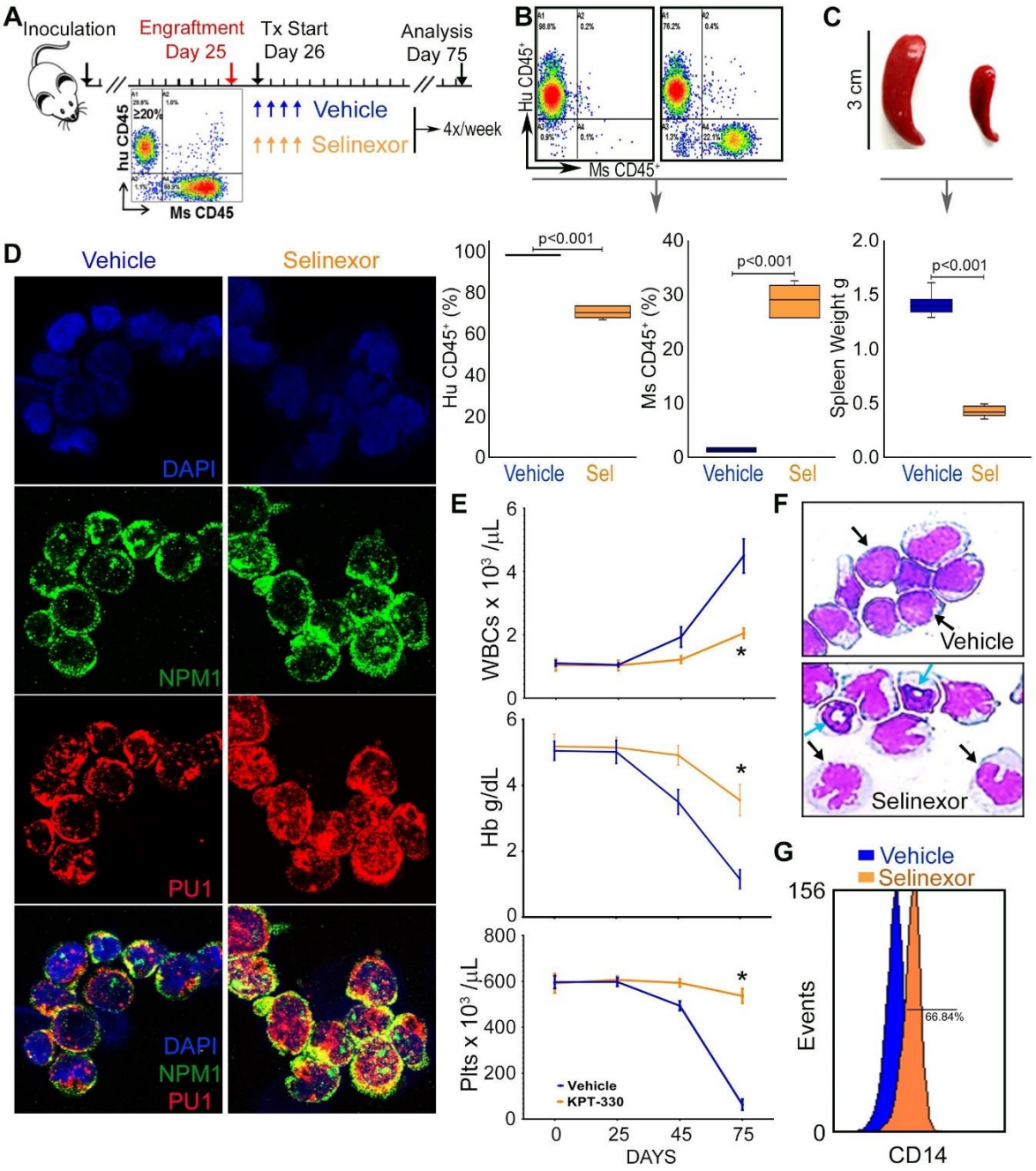

Figure S10. **Selinexor (KPT330) at a non-toxic dose significantly decreased AML burden in a patient-derived xenotransplant model of dual *NPM1*/*FLT3*-mutated AML**. **A) Experiment schema.** After confirmation of bone marrow leukemia engraftment to ≥20% in 3 randomly selected mice, remaining mice were randomized to vehicle versus selinexor 2 mg/kg starting on day 26 (n=6/group). Treatment continued until signs of distress in vehicle treated mice on day 75, at which point the experiment was terminated for analyses. **B) Bone marrow AML burden.** Flow cytometry for human CD45+ (AML) and murine CD45+ (normal) cells. Mean±SD. p-value t-test, 2-sided. **C) Spleen weights**. Mean±SD. p-value t-test, 2-sided. **D) Immunofluorescence for PU.1 and NPM1.** Bone marrow AML cells. DAPI was used to stain for nuclei. Images by Nikon Eclipse 400 microscope, magnification 630X. **E) Serial blood counts**. Increasing WBC were circulating myeloblasts. Tail-vein phlebotomy. Blood counts by HemaVet. Mean±SD, p-values 2-sided t-test selinexor-treated *vs* vehicle-treated at the time-point. **F) Bone marrow cell morphology.** Giemsa-stained. Black arrows: human AML cells (monocytic differentiated by selinexor); blue arrows: murine hematopoiesis. **G) CD14 expression on human AML cells from bone marrows of selinexor and vehicle treated mice**. Flow cytometry. Representative result from 1 mouse.

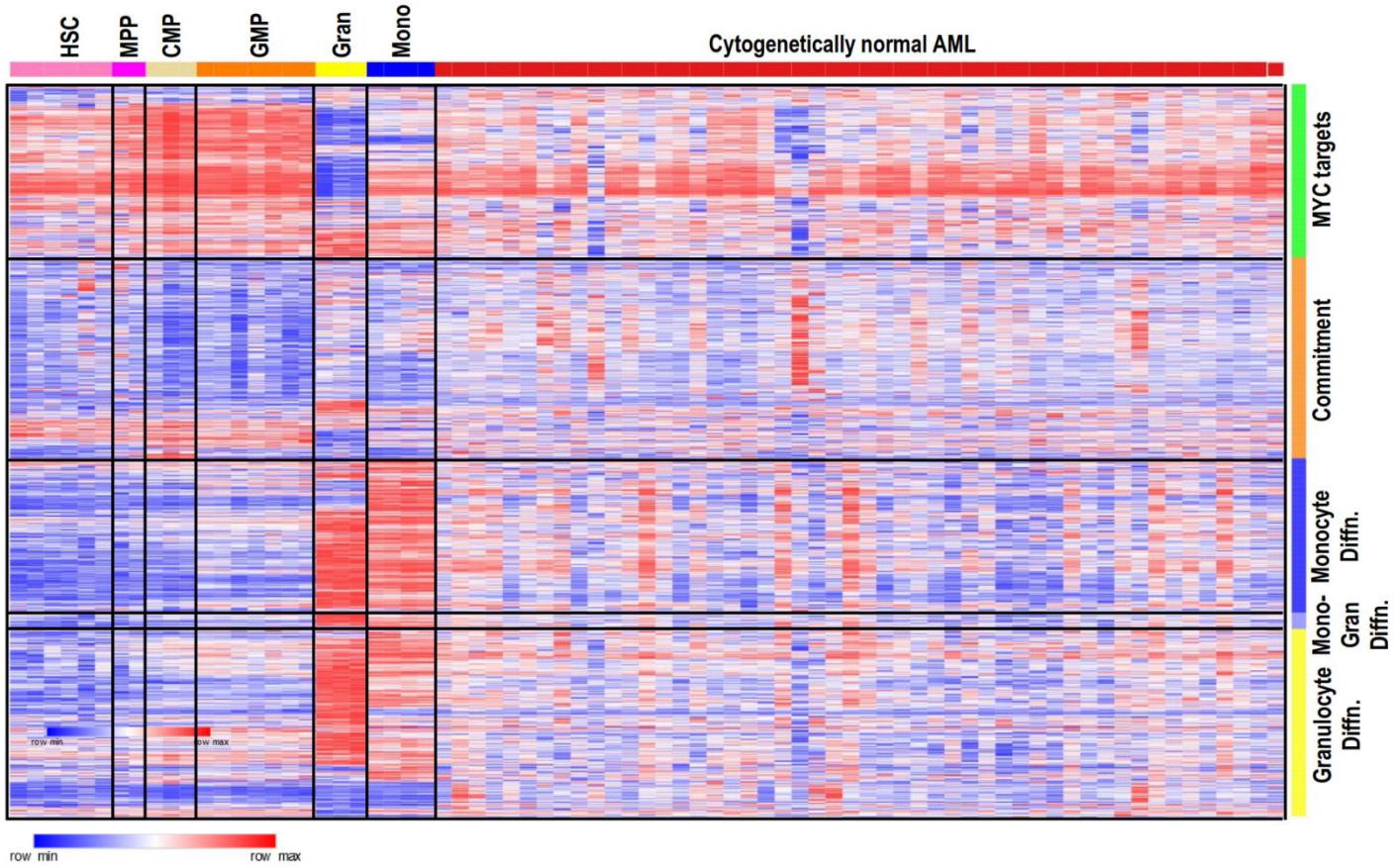

Figure S11. Monocyte and granulocyte terminal-differentiation genes, but not commitment/proliferation genes, are suppressed in cytogenetically normal AML cells (n=100) compared to normal granulocytes and monocytes, even though PU.1/CEBPA/RUNX1 master transcription factor expression resembled that of normal GMP/monocytes/granulocytes. Gene sets identified from a separate gene expression database as per figure 2 and Methods. Mono-Gran differentiation genes = genes common to both monocytes and granulocytes in those separate analyses.

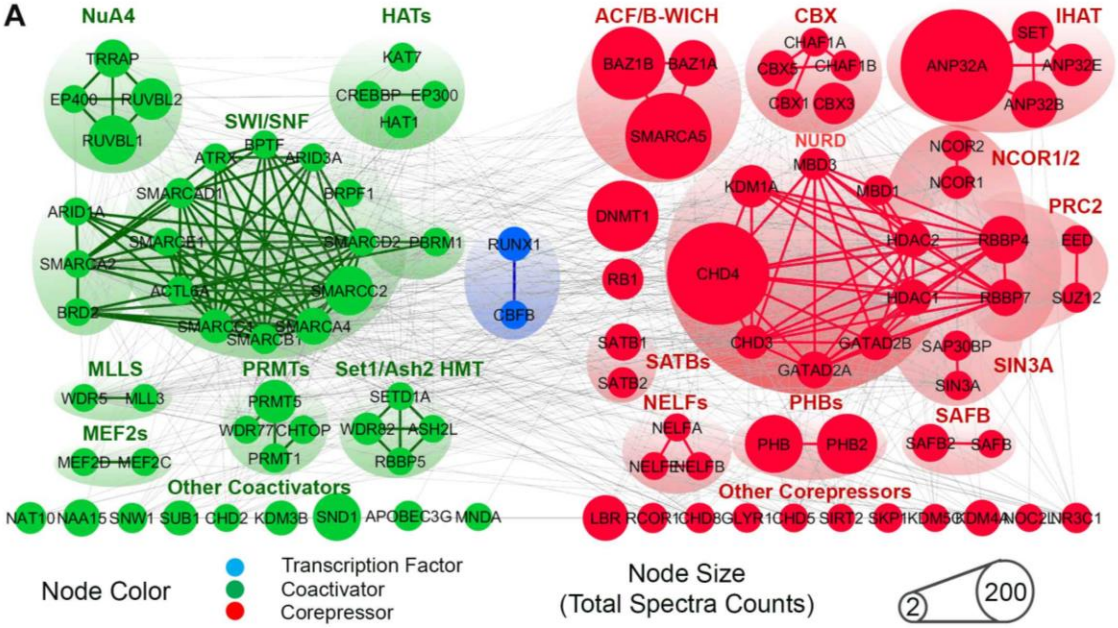

B

Function	ID	Veh	Dec	Sel
TF - Transcription Factors	RUNX1			
	CBFB			
Coactivators				
RMTs - Arginine Methyl Transferases	CHTOP			
	PRMT1			
	PRMT5			
	WDR77			
NuA4 complex	EP400			
	RBBP4			
	RBBP7			
	RUVBL1			
	RUVBL2			
	TRRAP			
SET1/ASH2 HMT	ASH2L			
	RBBP5			
	SETD1A			
	WDR82			
SWI/SNF	ACTL6A			
	ARID1A			
	ARID3A			
	ATRX			
	BPTF			
	BRD2			
	BRPF1			
	PBRM1			
	SMARCA2			
	SMARCA4			
	SMARCAD1			
	SMARCB1			
	SMARCC1			
	SMARCC2			
	SMARCD2			
	SMARCE1			
HATs - Other Histone Acetyltransferases	CREBBP			
	EP300			
	HAT1			
	KAT7			
MEFs	MEF2C			
	MEF2D			
MLL - H3K4 Methyl Transferase	KMT2C			
	WDR5			
	WDR61			
SAFBs	SAFB			
	SAFB2			
Other Coactivator	APOBEC3C			
	APOBEC3G			
	CHD2			
	KDM3B			
	MNDA			
	NAA15			
	NAT10			
	NCOA5			
	SND1			
	SNW1			
	SUB1			

Function	ID	Veh	Dec	Sel
Corepressors				
Corepressor	**DNMT1**			
Corepressor	**RB1**			
ACF/B-Wich	BAZ1A			
	BAZ1B			
	SMARCA5			
CBX / CAF1 Complex - H3K9 Methyl Transferase	CBX1			
	CBX3			
	CBX5			
	CHAF1A			
	CHAF1B			
IHAT - Inhibitor of Histone Acetyltransferases	ANP32A			
	ANP32B			
	ANP32E			
	NOC2L			
	SET			
NURD - Histone Deacetylase	CHD3			
	CHD4			
	GATAD2A			
	GATAD2B			
	HDAC1			
	HDAC2			
	KDM1A			
	MBD1			
	MBD3			
NCOR1/2	NCOR1			
	NCOR2			
SIN3	SAP30BP			
	SIN3A			
PRC2	EED			
	MORC3			
	SUZ12			
PHBs	PHB			
	PHB2			
SATBs	SATB1			
	SATB2			
NELF	NELFA			
	NELFB			
	NELFE			
Other Corepressors	RCOR1			
	GLYR1			
	KDM4A			
	SIRT2			
	CHD5			
	CHD8			
	HP1BP3			
	KDM5C			
	LBR			
	NR3C1			
	SKP1			

Figure S12. Coregulator interactions of nuclear RUNX1 in *NPM1*-mutated AML cells before and after DNMT1-depletion by decitabine or PU.1 nuclear retention by selinexor. Selinexor 20 nM or decitabine 0.25 μM was added to OCI-AML3 cells at 0 and 24 hours, and cells were harvested at 48 hours. Endogenous RUNX1 was affinity purified from nuclear fractions and coregulator interactions were analyzed by LCMS/MS. **A) RUNX1 interactions were skewed toward corepressors (coregulators that repress transcription), and away from coactivators that activate genes**. Quantification in Table S7. **B) Depletion of the corepressor DNMT1 by decitabine, or nuclear retention of PU.1 by selinexor, rebalanced toward coactivators**.

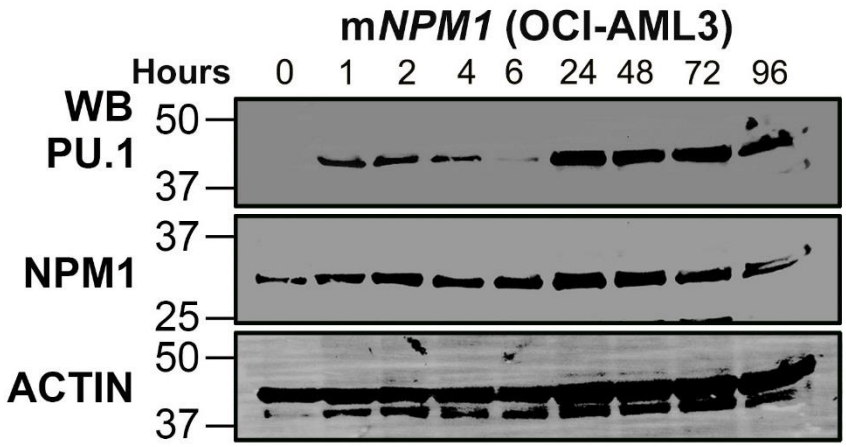

Figure S13. **DNMT1-depletion from *NPM1*-mutated AML cells by decitabine decreased NPM1 protein levels and increased PU.1 nuclear location.** Serial Western blots nuclear fractions of *NPM1*-mutated AML cells OCI-AML3 after treatment with decitabine 0.25 µM at 0 and 24 hours.

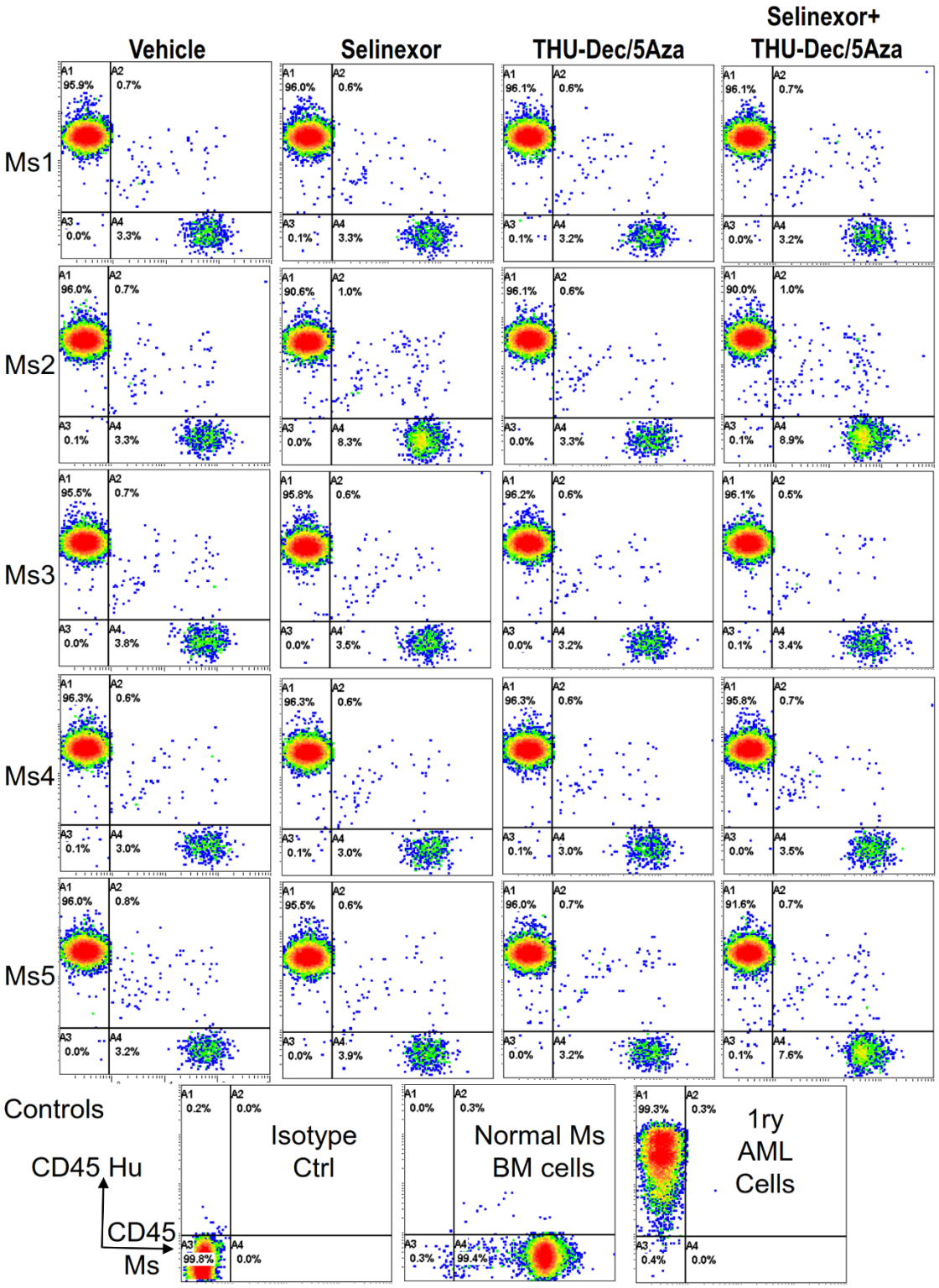

Figure S14. Human and murine CD45 expression in bone marrow cells obtained from mice at time-of-distress. Mice were treated with vehicle, selinexor, THU-decitabine/5-azacytidine, and the combination as per Figure 9. Ms 1-5 are the five individual mice per treatment group. Isotype controls and single-staining for human CD45 in human AML cells and normal murine bone marrow also shown. Measurements by flow-cytometry.

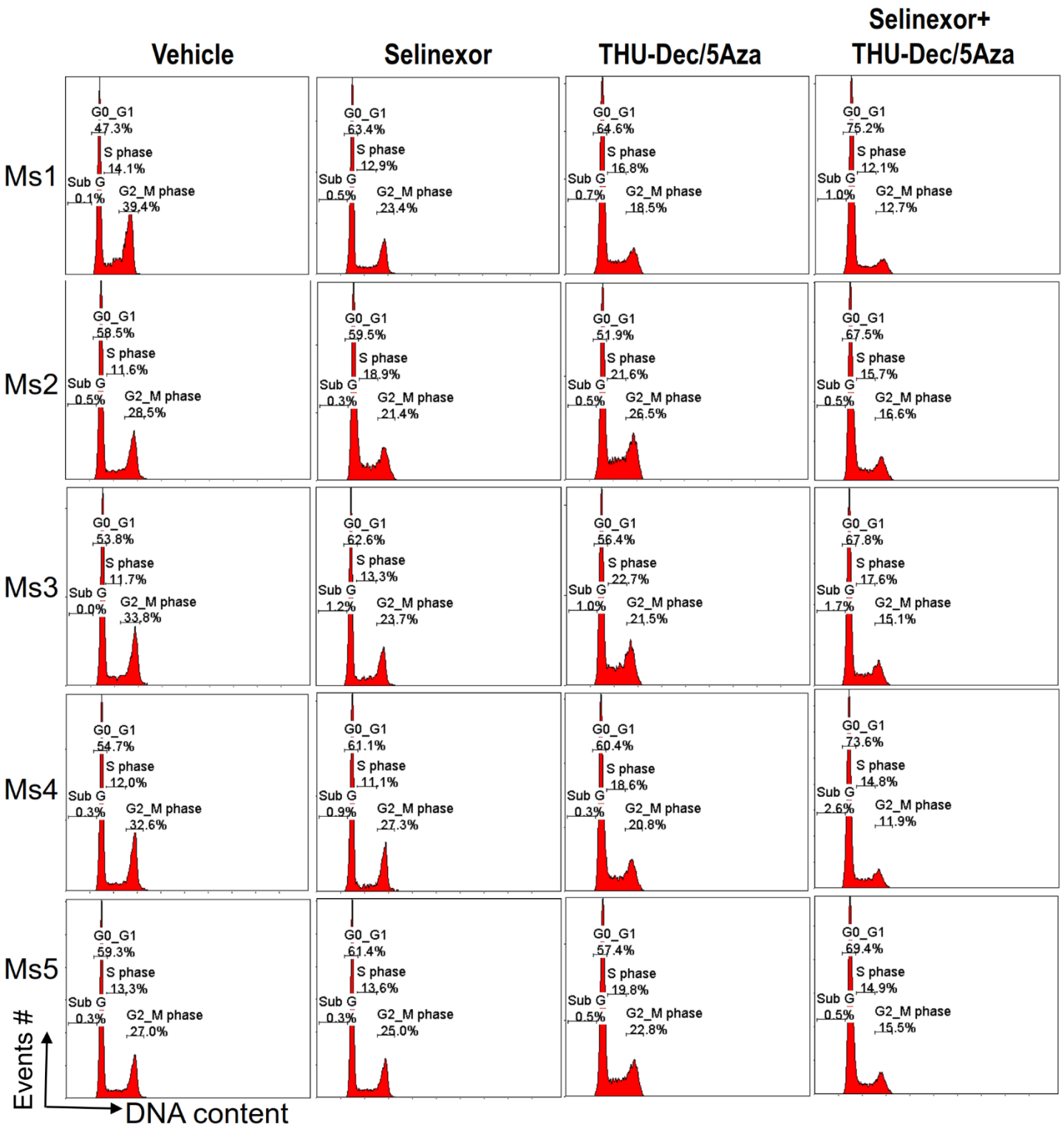

Figure S15. Cell cycle distribution of bone marrow AML cells obtained from mice at time-of-distress. Mice were treated with vehicle, selinexor, THU-decitabine/5-azacytidine, and the combination as per Figure 9. Ms 1-5 are the five individual mice per treatment group. DNA content measured by propidium-iodide staining and flow cytometry.

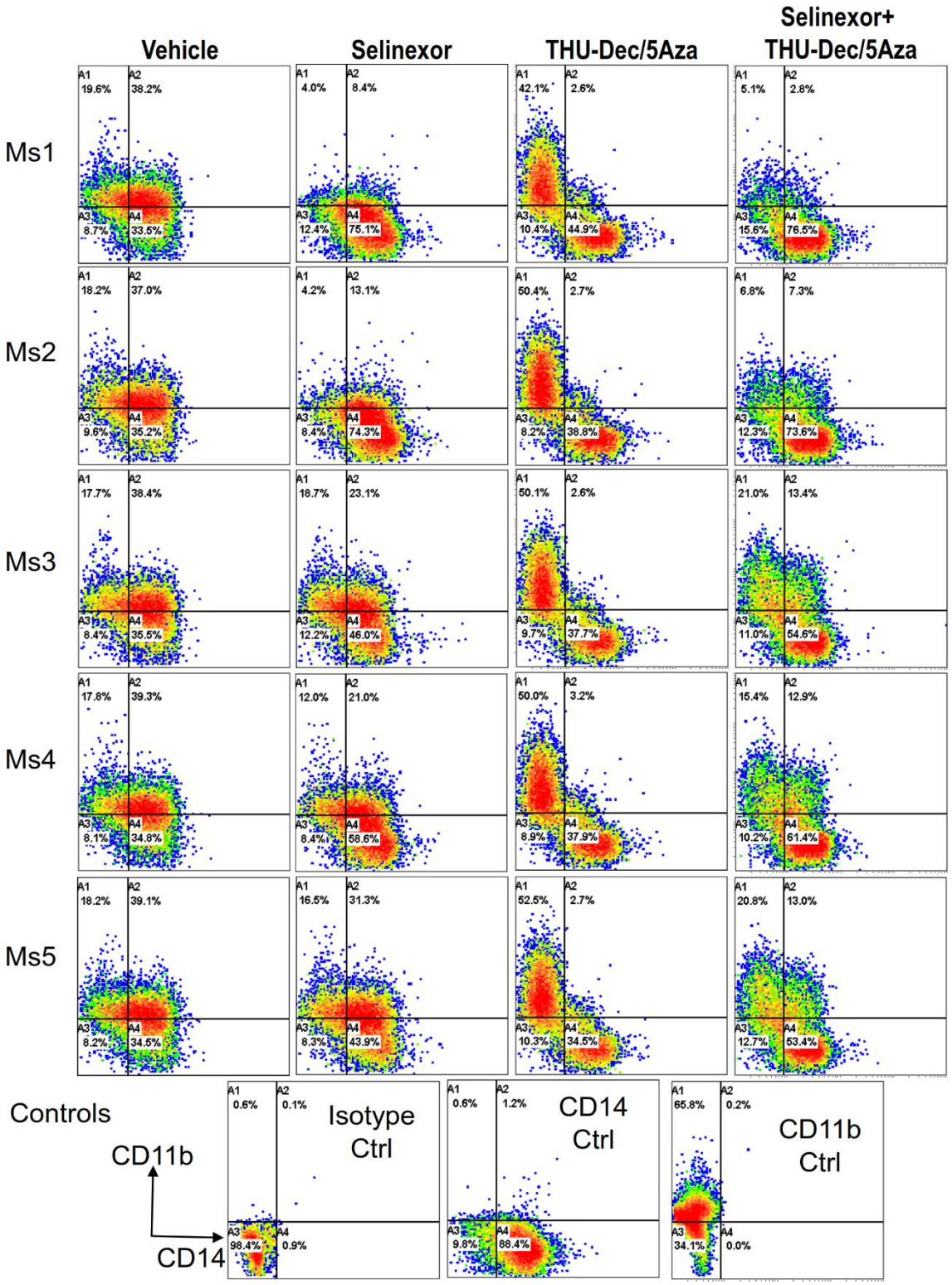

Figure S16. Monocyte (CD14) and granulocyte (CD11b) lineage-differentiation marker expression in bone marrow cells obtained from mice at time-of-distress. Mice were treated with vehicle, selinexor, THU-decitabine/5-azacytidine, and the combination as per Figure 9. Ms 1-5 are the five individual mice per treatment group. Isotype controls and single-staining for human CD45 in human AML cells also shown. Measurements by flow cytometry.

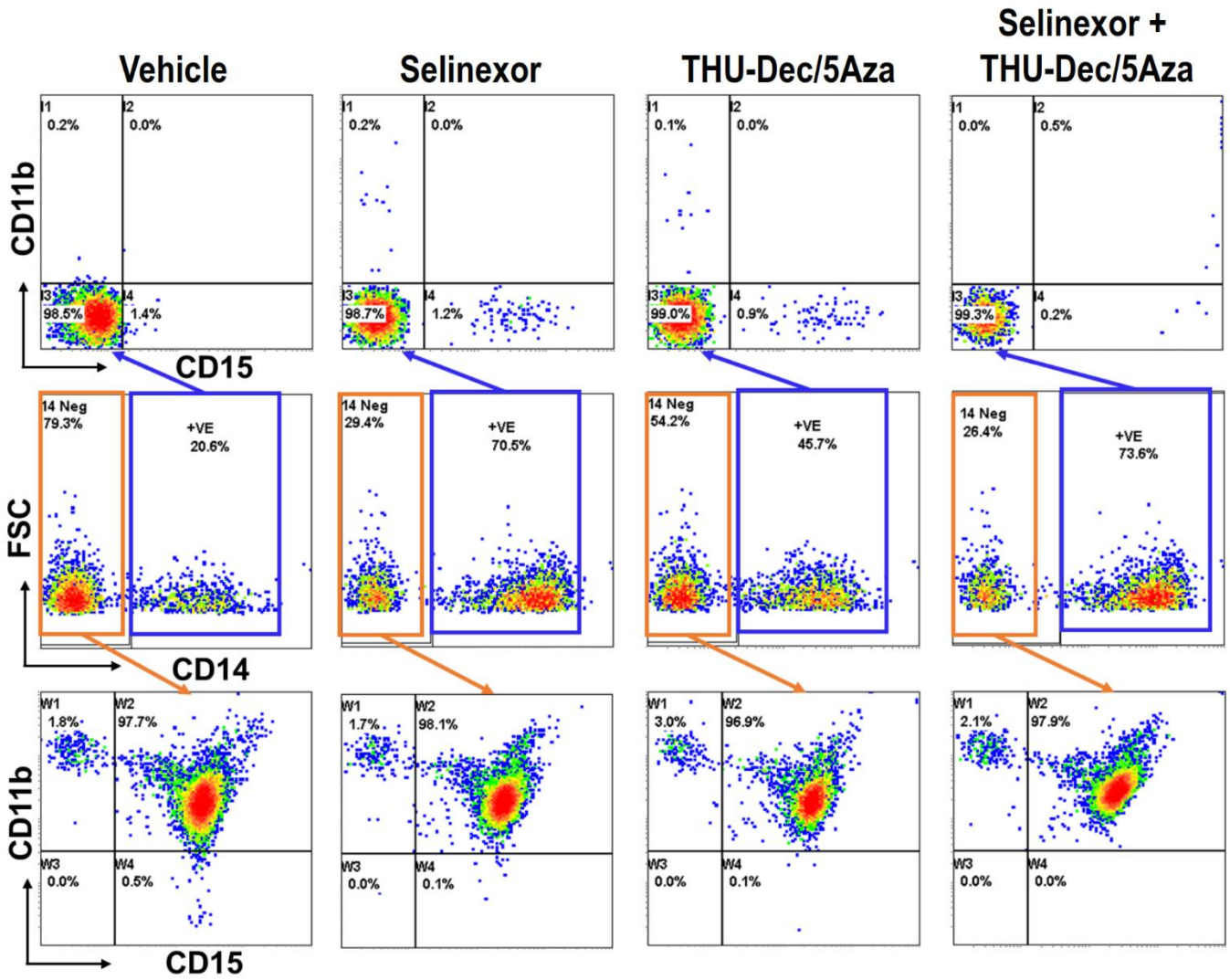

Figure S17. CD14-positive *NPM1*-mutated AML cells did not stain for CD11b or CD15 (monocytic), while CD14-negative *NPM1*-mutated AML cells co-stained for CD11b and CD15 (granulocytic). AML cells from bone marrow harvested at time-of-euthanasia of the mice receiving vehicle, selinexor alone, THU-decitabine/5-azacytidine, or the combination treatment (experiment shown in **Figure 9**), were stained in the same tube for CD11b, CD15 and CD14. CD14 negative cells were positive for both CD11b and CD15 (granulocytic), while CD14 positive cells were negative for both CD11b and CD15 (monocytic).

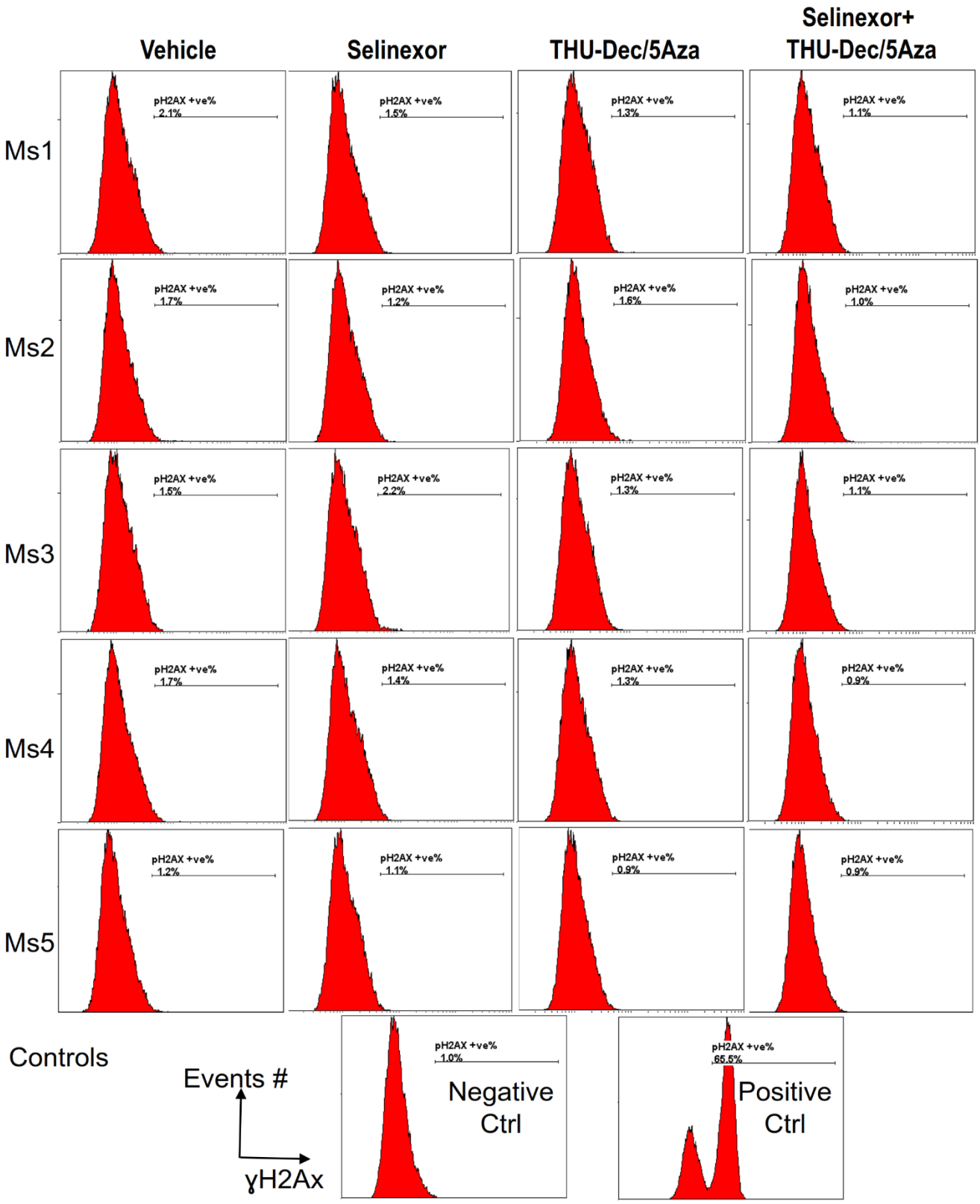

Figure S18. γ-H2AX expression as a marker for apoptosis/DNA damage in bone marrow cells obtained from mice at time-of-distress. Mice were treated with vehicle, selinexor, THU-decitabine/5-azacytidine, and the combination as per Figure 9. Ms 1-5 are the five individual mice per treatment group. Positive control was generated by treating cells with camptothecin 10 µM overnight. Measurements by flow cytometry.

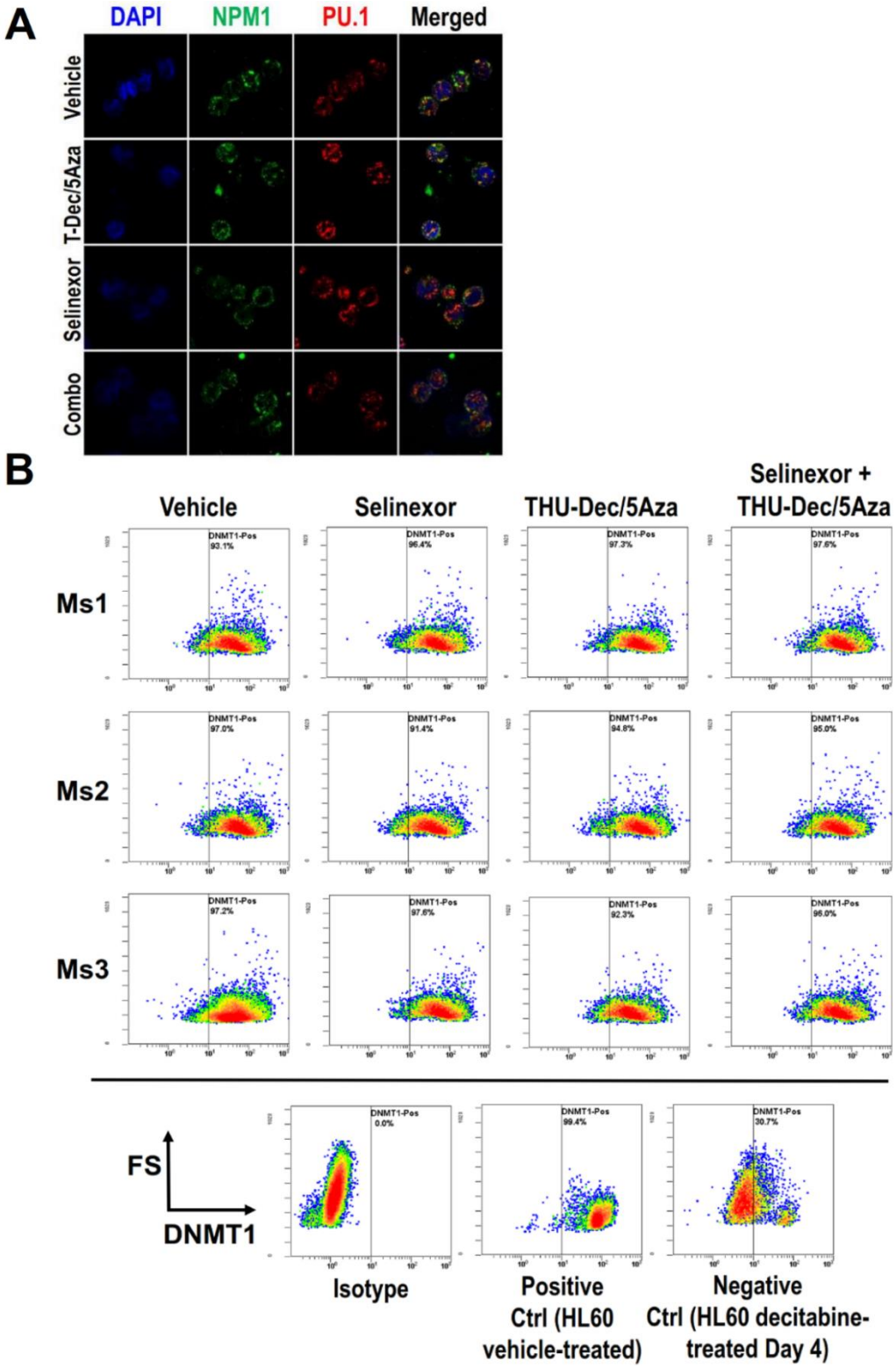

Figure S19. Resistance both in vivo and in vitro was by preventing selinexor-induced mutant-NPM1/PU.1 nuclear relocation, and decitabine/5-azacytidine-induced DNMT1-depletion. A) NPM1 and PU.1 localization in *NPM1*/*FLT3*-mutated AML cells harvested from murine bone marrow at the time-of-distress (experiment from Figure 9). Immunofluorescence microscopy for PU.1 and NPM1, DAPI was used to stain for nuclei. Images by Leica SP8 inverted confocal microscope, magnification 630X. Bone marrow from 1 mouse per treatment group was analyzed. **B) DNMT1 content of the AML cells**. DNMT1 measured by flow cytometry. Bone marrows from 3 mice per treatment group were analyzed.